Crack Bridging by Uncracked Ligaments during Fatigue-Crack Growth in SiC-Reinforced Aluminum-Alloy Composites

JIAN KU SHANG and R.O. RITCHIE

Micro-mechanisms of crack-tip shielding associated with the growth of fatigue cracks in metal-matrix composites are examined with specific emphasis on the role of crack bridging by uncracked ligaments. Simple analytical models are developed for such bridging induced by both overlapping cracks and by coplanar ligaments in the wake of the crack tip; the models are based on respective notions of a critical tensile strain or critical crack-opening displacement in the ligament. The predicted degree of shielding derived from these mechanisms is not large, but is found to be consistent with experimental observations in high-strength P/M aluminum alloys reinforced with 15 to 20 vol pct of SiC particulate.

I. INTRODUCTION

RECENT studies in a wide range of metallic and nonmetallic materials have demonstrated the role of crack-tip shielding in enhancing toughness, or more generally in impeding crack advance, by locally reducing the crack driving force actually experienced at the crack tip; notable examples are transformation-toughening in ceramics, rubber-toughening in polymers, and fatigue-crack closure in metals, as reviewed in References 1 and 2. In certain materials, particularly ceramic composites, a prominent shielding mechanism occurs by bridging between the crack faces;[3–17] such bridges can be generated by the presence of brittle fibers,[3–8] ductile particles,[9–12] or unbroken ligaments in the wake of the crack tip.[13–17]

The dominant contribution to toughening from bridging reinforcements can be expressed simply as the product of the volume fraction of the bridging phase with the area under the stress/strain curve, *i.e.*, in terms of the yield strength, σ_y, radius R_f, and volume fraction V_f of the reinforcement phase:[11]

$$G_c = C\sigma_y R_f V_f \qquad [1]$$

where C depends on the ductility of the reinforcement phase and the extent of interface debonding. In brittle fiber-reinforced ceramic-matrix composites, such as SiC fibers in alumina where the fibers are sufficiently strong and the fiber/matrix interface sufficiently weak, preferential failure in the matrix can leave intact fibers spanning the crack for some distance behind the crack tip; as the crack opens, fiber motion then is restrained, for example, by friction in the interface.[1,3–8] With ductile-phase reinforcements, such as rubber in polymers or aluminum particles in alumina, particles in the crack path can similarly act as bridges and contribute to the toughness by exhibiting extensive plastic stretching in the crack wake.[9–12] In either case, the reinforcement phase, provided it remains unbroken and is intercepted by the crack, can act as a series of springs which restrain crack opening and thereby shield the crack tip from the applied far-field loading, resulting in lower, yet crack-size dependent, growth-rate behavior.[3–8]

In metallic materials, similar bridging effects are developed in aluminum-alloy laminates reinforced with epoxy-resin sheets impregnated with unidirectional aramid fibers (ARALL®* Laminates), where the fiber/epoxy interfaces now are weak enough to permit controlled delamination and, thus, bridging of unbroken fibers across the crack.[18,19] However, in most metal-matrix composites, such as aluminum alloys discontinuously reinforced with SiC fibers (or whiskers or particles), the reinforcement phase invariably fractures due to its strong interface with the matrix, with the result that particle or fiber-bridging essentially is insignificant.[17,20]

Recently, however, studies on fatigue-crack growth in aluminum alloy/SiC-particulate composites (Al/SiC_p) have revealed a different mechanism of bridging, induced by the presence of uncracked ligaments behind the crack tip.[17] Such ligaments, although not necessarily continuous in three dimensions, act in any one two-dimensional section to inhibit crack opening. This mechanism also has been reported for carbide-initiated cleavage cracking in steels[15,16] and from selective fracture of preferential grains in polycrystalline alumina.[13] Mechanistically, it appears to result from fracture events triggered ahead of the crack tip or from general non-uniform or discontinuous advance of the crack front; in Al/SiC_p composites, it predominates at intermediate fatigue-crack growth rates ($\sim 10^{-9}$ to 10^{-6} m/cycle), where cleavage of SiC particles ahead of the crack tip becomes significant.[17]

The objective of the present study is to characterize the nature and significance of such uncracked-ligament bridging in Al/SiC_p composites and to derive simple models to quantify the magnitude of the induced shielding.

*ARALL Laminate is a registered trademark of the Aluminum Company of America.

II. EXPERIMENTAL PROCEDURES

The metal-matrix composites used in this investigation were based on a powder-metallurgy (P/M) Al-Zn-Mg-Cu matrix alloy; the alloy, designated Alcoa MB78, is

JIAN KU SHANG, Research Assistant, and R.O. RITCHIE, Professor, are with the Department of Materials Science and Mineral Engineering at the University of California, Berkeley, CA 94720.

Manuscript submitted April 15, 1988.

similar to 7091 with composition shown in Table I. Reinforcement was provided by a nominal 15 or 20 vol pct of silicon carbide particulate of either coarse F-600 grade (nominal size 16 μm) or fine F-1000 grade (nominal size 5 μm). The composite alloys were fabricated by blending prealloyed atomized aluminum-alloy powders with SiC particles, compacting by cold isostatic pressing, vacuum degassing and hot pressing to roughly theoretical density, and, finally, extruding at an extrusion ratio of 12:1 into 25-mm-thick plates;[21] the unreinforced (control) alloy was fabricated in similar fashion, but naturally without the SiC.

In the present study, the alloys (both unreinforced and reinforced) were examined in an overaged condition. The extruded plates were solution treated 4 hours at 530 °C, quenched in cold water, and (owing to large differences in thermal expansion between the matrix and carbide) immediately compressed 2 to 3 pct by forging to produce a uniform state of deformation to minimize quenching-induced residual stresses. Subsequent aging was performed for 24 hours at 121 °C followed by 50 hours at 171 °C (T7X2 temper). Room-temperature uniaxial tensile properties (transverse direction) and fracture-toughness values (S-T orientation) are listed in Table II.

Optical micrographs of the microstructures are shown in Figure 1. Transmission electron microscopy revealed precipitation of η' ($MgZn_2 \cdot Mg(CuAl)_2$) platelets and equilibrium $\eta(MgZn_2)$ in the matrix, and smaller (~0.1 μm) η precipitates on SiC/matrix interfaces. Average SiC particle sizes (aspect ratio ~3:1) were found to be 11.4 μm in the 15 vol pct alloy and 6.1 μm in the 20 vol pct alloy; grain sizes varied between 2.3 and 4.8 μm. In the 15 vol pct alloy with coarse SiC particles, the distribution of particle sizes was more uniform (Weibull modulus of 2.6) than in the 20 vol pct alloy with finer SiC, where distinct clustering of particles was evident (Weibull modulus of 1.6). Further details on the microstructure and particle-size distributions for these materials are given in References 17 and 21.

Fatigue-crack propagation tests were performed using 6.4-mm-thick double-cantilever-beam $DB(M_z)$ specimens (S-T orientation), cycled in controlled room air (22 °C, 45 pct relative humidity) at a load ratio ($R = K_{min}/K_{max}$) of 0.1 and a frequency of 50 Hz (sine wave), in general accordance with the guidelines suggested by ASTM Standard E 647-86A. Results were obtained under automated stress-intensity control (with a normalized K-gradient of -0.2 per mm) over a wide spectrum of growth rates from 10^{-12} to 10^{-5} m/cycle, using d.c. electrical-potential methods to monitor crack advance. Stress intensities were computed using the linear-elastic solutions of Srawley and Gross.[22] The extent of crack closure was evaluated from crack-mouth opening displacement measurements to determine a closure stress intensity, K_{cl}, defined at first contact of the crack surfaces on unloading.[23] Using such measurements, fatigue-crack growth rate data are presented as a function of both the nominal (applied) stress-intensity range, $\Delta K = K_{max} - K_{min}$, and the effective stress-intensity range, $\Delta K_{eff} = K_{max} - K_{cl}$, which allows for the shielding effect of closure.

Fracture morphology was examined in the scanning electron microscope and from crack-path profiles, obtained from metallographic sections (at specimen mid-thickness) on cracks previously impregnated with epoxy. To ensure that uncracked ligaments indeed were uncracked, specimens used for crack profiles were wedge-open loaded to a crack-opening displacement equivalent to $K \approx 10$ MPa$\sqrt{m}$ prior to sectioning. Metallographic sections also were taken at other points along the crack front to reveal the three-dimensional morphology of the crack.

III. EXPERIMENTAL RESULTS

Fatigue-crack propagation rates (da/dN), as a function of both the nominal and effective stress-intensity ranges (ΔK and ΔK_{eff}) for both Al/SiC_p composites, are plotted over a wide spectrum of growth rates from 10^{-12} to 10^{-5} m/cycle in Figure 2 and are compared with results for the unreinforced matrix alloy; data are presented in terms of ΔK_{eff} to remove confusing effects from shielding by crack closure. Based on metallographic sectioning, uncracked ligaments in the wake of the crack tip (Figure 3) were evident primarily in the intermediate growth-rate regime, between typically 10^{-9} and 10^{-6} m/cycle. However, before describing the bridging effect, it is pertinent first to briefly describe behavior in the other regimes.

As discussed elsewhere for peak-aged microstructures,[17] fatigue-crack growth behavior in Al/SiC-particulate composites can be categorized into three regimes. At near-threshold levels below typically 10^{-9} m/cycle, crack closure is the predominant shielding mechanism. This is confirmed in Figure 2 by the close correspondence below $\sim 10^{-9}$ m/cycle between crack-growth rates for reinforced and unreinforced alloys, when closure is subtracted out, *i.e.*, when results are plotted as a function of ΔK_{eff}. In certain microstructures, the crack has a tendency to avoid SiC particles; intrinsic fatigue thresholds, $\Delta K_{TH,eff}$, are generally higher than for the unreinforced constituent matrix, which in part is reflective of the higher stiffness and, hence, smaller crack-tip opening displacements (at a given ΔK) in the composite alloys. With increasing ΔK level, the crack starts progressively to seek out SiC particles ahead of the crack tip, consistent with the increase in plastic-zone size and, hence, statistical sampling volume. This results in an increasing tendency (with increasing ΔK) for the premature fracture of SiC ahead of the crack tip which, because of imperfect coalescence of these cracks with the main crack tip, in turn leads to nonuniform crack fronts, the production of uncracked ligaments, and, hence, to

Table I. Chemical Composition (in Wt Pct) of Matrix Al-Zn-Cu Alloy

Zn	Cu	Mg	Si	P	S	Zr	Al
9.44	2.50	3.33	0.14	0.14	0.17	0.08	balance

Table II. Room-Temperature Tensile Properties of Overaged (T7X2) Alloy

Alloy	Yield Strength σ_y (MPa)	Tensile Strength (MPa)	Elongation on 13 mm (Pct)	Reduction in Area (Pct)	K_{Ic}* (MPa$\sqrt{m}$)
MB78 unreinforced	380	452	11.9	44.5	46.0#
MB78 + 15 pct coarse SiC_p	405	460	3.2	10.5	16.6
MB78 + 20 pct fine SiC_p	393	439	2.1	9.1	14.3

*S-T orientation.
#Invalid result.

shielding from crack bridging. Thus, growth rates in this intermediate regime are progressively slower in reinforced alloys, although the effect in certain microstructures, *e.g.*, the 20 vol pct fine SiC_p composite, can be minimal (Figure 2). Conversely, at higher ΔK levels above $\sim 10^{-6}$ m/cycle, growth rates become faster in the composites; this behavior represents the acceleration in growth rates characteristic of stress-intensity levels which approach instability and reflects the far lower fracture toughness of the reinforced alloys.

IV. EVIDENCE FOR CRACK BRIDGING

In the present Al/SiC_p composites, two distinct types of ligament bridging have been observed during fatigue-crack propagation at intermediate stress intensities. In the alloy with a higher SiC volume fractions and small interparticle spacings (20 vol pct fine SiC_p), the uncracked ligaments are predominantly coplanar with the crack and directly associated with fracture of carbides ahead of the crack tip (Figure 3(a)). In addition, because of their limited size, few SiC particles are present in the ligament. By comparison to behavior in the unreinforced alloy, the resulting effect on crack-growth rates from this form of bridging is small (Figures 2(a) and (b)). Conversely, in alloys with lower volume fractions of more dispersed SiC particles (15 vol pct coarse SiC_p), the uncracked ligaments are formed principally by overlapping cracks on different planes (Figure 3(b)), with the result that the beneficial effect on growth rates is now considerably larger (Figures 2(c) and (d)).

As noted above, the creation of uncracked ligaments appears to result from nonuniform growth of the crack front, promoted by the fracture of SiC particles ahead of the crack tip. This is illustrated in Figure 4, where the microcracks created ahead of the tip are clearly associated with cracked particles. Akin to the analogous fracture of iron carbides during cleavage fracture in steels,[24] the particle cracking process may be considered to be stress-controlled and, therefore, triggered at sites *ahead* of the crack tip where the tensile stresses are highest (due to crack-tip blunting at the crack tip).* This

*Based on the asymptotic crack-tip solutions for a power-hardening solid by Hutchinson, Rice, and Rosengren,[25,26] modified by the blunting solutions of Rice and Johnson[27] and McMeeking,[28] the maximum tensile stresses peak at some two crack-tip opening displacements ($\sim K^2_{max}/\sigma_y E$) directly ahead of the crack tip.

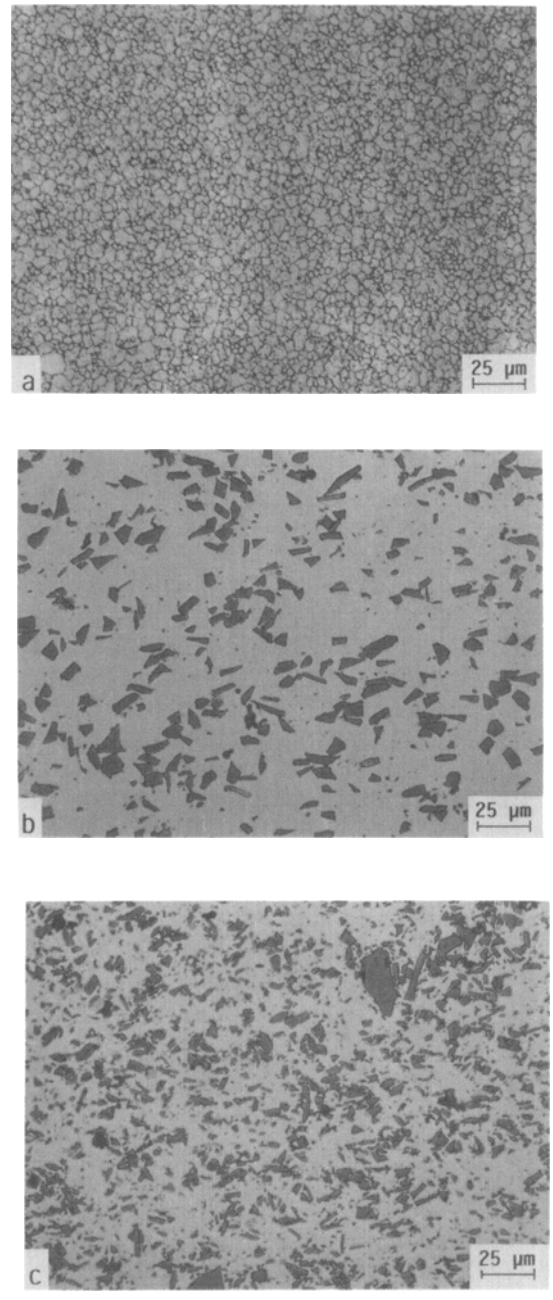

Fig. 1—Optical micrographs of the overaged microstructures of (*a*) unreinforced matrix alloy; (*b*) 15 vol pct coarse Al/SiC_p composite; and (*c*) 20 vol pct fine Al/SiC_p composite.

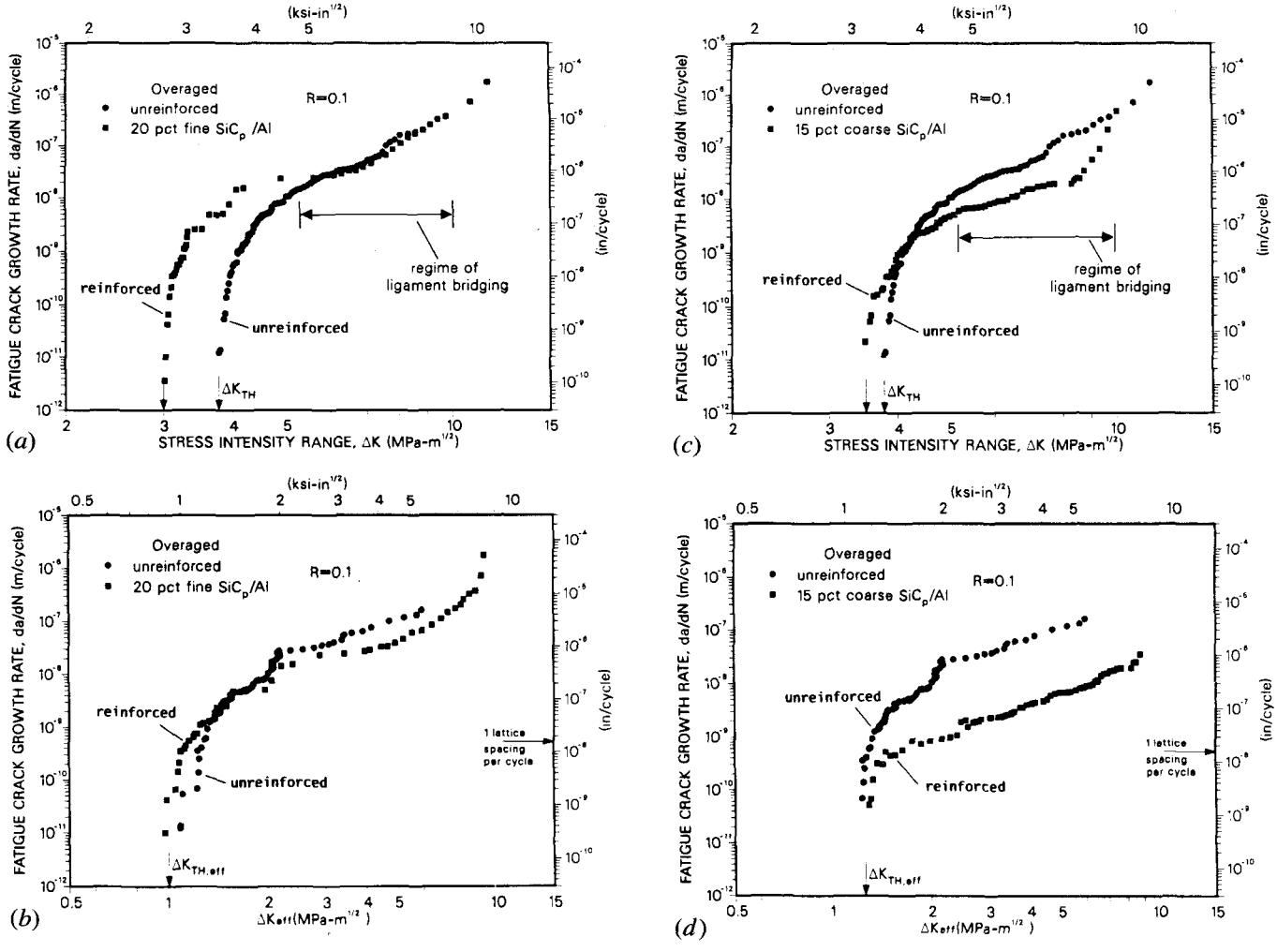

Fig. 2—Variation in fatigue-crack growth rates, da/dN, with nominal and effective stress-intensity ranges, ΔK and ΔK_{eff}, for (*a*) and (*b*) 20 vol pct fine Al/SiC_p composite; (*c*) and (*d*) 15 vol pct coarse Al/SiC_p composite, compared to corresponding behavior in unreinforced constituent-matrix alloy. Crack bridging in Al/SiC_p predominates over the range ($\sim 10^{-9}$ to 10^{-6} m/cycle). Growth-rate differences at low ΔK levels are seen to be associated primarily with crack closure; no bridging is observed in this regime.

mechanism is promoted at higher stress intensities because at low ΔK levels, where the plastic zone and, hence, region of high stresses ahead of the tip (*i.e.*, process zone) is small, the probability of finding a weak (eligible) particle which will crack is limited due to the small sampling volume; with increasing ΔK levels, the process zone and, hence, sampling volume increase rapidly such that the probability of finding an eligible particle is much enhanced.[17]

Not all microcracks in Figures 3 and 4 appear to be associated with a cracked particle; furthermore, they are generally much larger than the particle size. This follows because the population of particles cracked ahead of the tip is not large (as in low-temperature cleavage fracture of steels[29,30]) such that, in any one two-dimensional micrograph, the particle microcrack itself may not be sectioned. However, depending upon the size and orientation of the microcrack, the stress intensity at the tip nearest to the original crack tip may be as high as 74 pct of the applied K on the original crack,[31–34] such that growth of the microcrack invariably will occur. In general, several microcracks are formed ahead of the main crack tip (Figures 3 and 4); analysis describing the respective stress distributions and stress intensities generated at their tips is outlined in the appendix.

V. MODELING OF CRACK BRIDGING

There have been several previous models to evaluate the role of crack bridging in metals, ceramics, and composites;[3–18] in essence, the key problem lies in defining the force in the bridges as a function of the crack-opening displacement or distance from the crack tip. A listing of the force-separation functions utilized in five prominent models[5,9,14–16] is given in Table III. The fiber-bridging model of Marshall *et al.*[5] and the rubber-particle toughening model of Kunz-Douglass *et al.*[9] compute the strain in the bridges from the strain compatibility between the fiber and matrix during fiber pullout or from the shape change of rubber particles and thus are mechanism-specific. Conversely, Mai and Lawn,[14] in their interfacial-bridging model for toughness and resistance-curve behavior in ceramics, simply adopt a trial exponential force-separation function, with parameters set by the

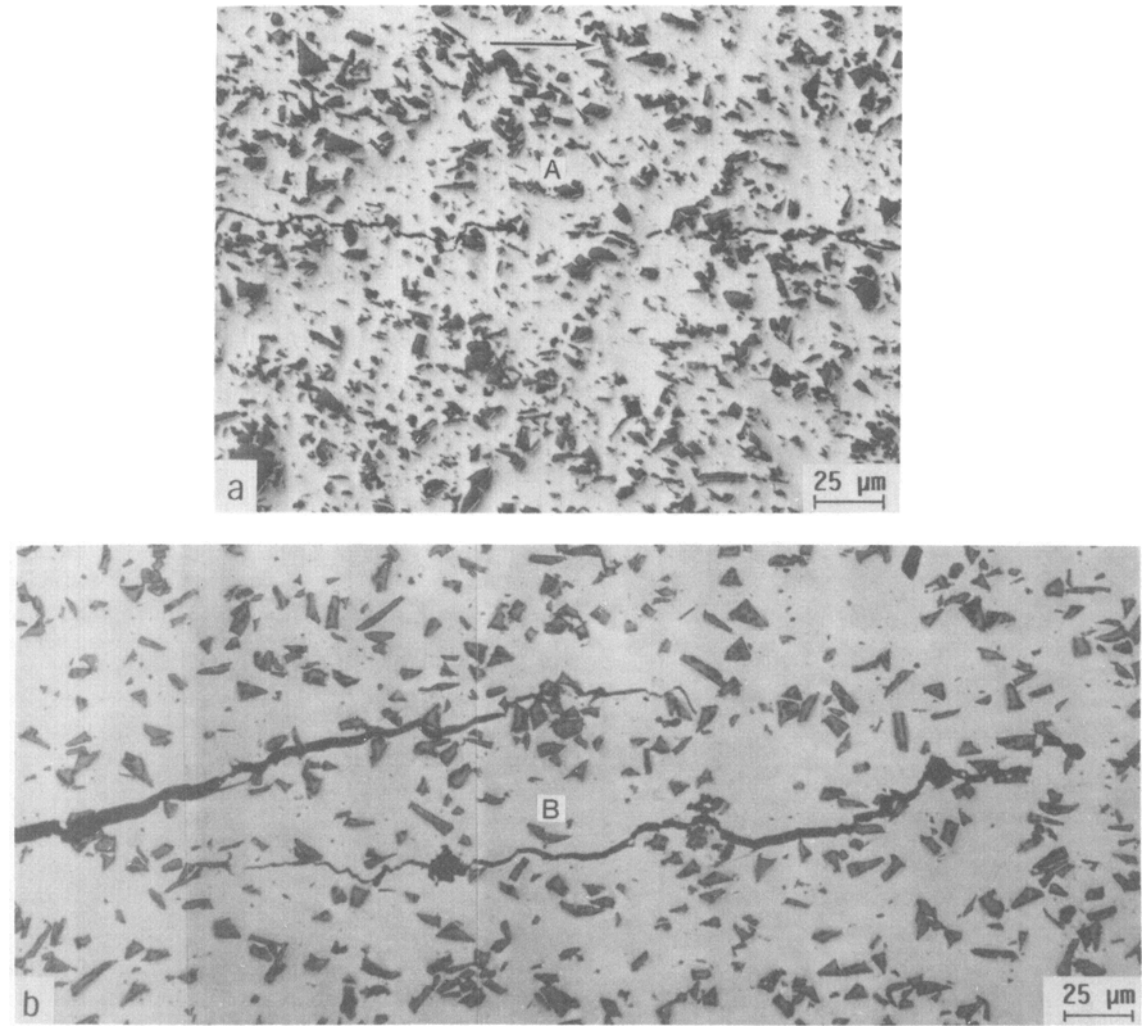

Fig. 3—Uncracked-ligament bridging in Al/SiC_p composites, showing (*a*) coplanar ligaments in 20 vol pct fine Al/SiC_p composite (region A); (*b*) overlapping ligaments in 15 vol pct coarse Al/SiC_p composite (region B). Horizontal arrow indicates general direction of crack growth.

particular mechanism. The equilibrium-crack models of Gerberich[15] and Rosenfield and Majumdar,[16] on the other hand, are more general, but assume simply that the stress in the bridges is equal to the yield or fracture stress, respectively.

In the current work, two approaches are taken to model the forms of ligament bridging observed during fatigue-crack growth in Al/SiC_p, *i.e.*, based on a limiting crack-opening displacement or a limiting strain in the uncracked ligaments; analyses are described below.

A. *General Considerations*

The uncracked ligaments are taken to exist over a distance $x = \ell$ (the bridging zone) behind the crack tip and are characterized by area fraction, f, occupied on the crack plane (Figure 5). The ligaments act as bridges which limit crack opening; consequently, the stresses introduced into these ligaments depend upon the opening displacements of the crack faces. The resulting restraining effect thus can be represented by forces exerted on the crack faces, which are a function of the stresses in the ligament and the ligament size. As the distribution and size of the ligaments are a complicated function of local microstructure, for simplicity, a uniform distribution is assumed such that the distributed force per unit thickness, $dp(x)$, from uncracked ligaments in an infinitesimal interval, dx, can be represented as:

$$dp(x) = f\sigma(x)\, dx \qquad [2]$$

where $\sigma(x)$ is the stress in the ligaments. For a semi-infinite crack, this distributed force induces a stress intensity given by:[35]

$$K_s = \frac{\sqrt{2}}{\pi} \int_0^{\ell} \frac{dp(x)}{\sqrt{x}} \qquad [3]$$

If the crack is now subjected to an applied stress field σ_a, superposition of the shielding stress intensity, K_s, due to bridging with the globally applied (far-field) stress intensity, K_a, yields an expression for the effective (near-tip) stress intensity, K_{tip}, experienced locally at the crack tip:

$$K_{tip} = K_a + K_s \qquad [4]$$

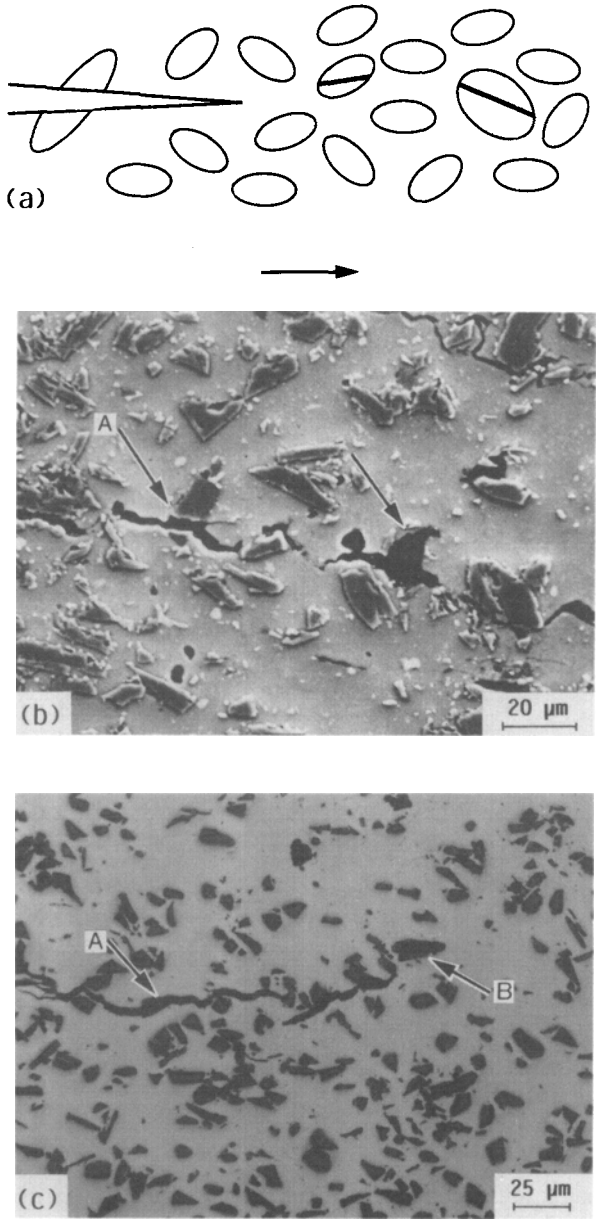

Fig. 4—Evidence for the creation of uncracked ligaments in Al/SiC_p composites resulting from SiC fracture, both ahead (location B) and in the wake (location A) of the crack tip (indicated by inclined arrows). Shown are (*a*) schematic illustration of the cracking process; and bridging from (*b*) coplanar uncracked ligaments in 20 vol pct fine Al/SiC_p composite; and (*c*) overlapping ligaments in 15 vol pct coarse Al/SiC_p composite. Horizontal arrow indicates general direction of crack growth.

Solutions to Eqs. [2] through [4], involving the determination of the stress function $\sigma(x)$, are given below.

B. *Limiting Crack-Opening Displacement Approach*

The basis of this approach is that the stress in any ligament behind the crack tip is related to the crack opening at that point; specifically, the displacement in the last intact ligament at the end of the bridging zone must approach the limiting crack-opening displacement, δ_c, for fracture of that ligament. By assuming for simplicity that an idealized fatigue crack can be taken as trapezoidal (Figure 6), the crack-opening displacement, δ_x, at any distance x along the crack length can be determined in terms of the crack-tip opening displacement, δ_{tip}, and specimen ligament, b:[36]

$$\delta_x = \delta_{tip}\left(\frac{x + rb}{rb}\right) \qquad [5]$$

assuming that the crack opens about some rotational axis at a distance, rb, ahead of the crack tip; r is the rotational factor and takes values between 0.195 for elastic deformation and 0.470 for plastic deformation.[37] The value of the crack-tip opening displacement, δ_{tip}, can be determined from near-tip stress intensity, K_{tip}, in terms of Young's modulus, E, and the yield strength, σ_y, of the ligament:[38]

$$\delta_{tip} = d \cdot \frac{K_{tip}^2}{E'\sigma_y} \qquad [6]$$

where $E' = E$ in plane stress and $E/(1 - \nu^2)$ in plane strain, ν is Poisson's ratio, and d is a constant varying between 0.3 and 1.0, depending upon the yield strain and work-hardening exponent and whether plane-strain or plane-stress conditions apply.[38]

To maintain equilibrium such that the crack may extend without breaking ligaments along the bridging zone, the crack-opening displacement at any point within the zone, δ_x, must satisfy:

$$\delta_x \leq \delta_c, \qquad 0 \leq x \leq \ell \qquad [7a]$$

whereas at the end of the bridging zone:

$$\delta_x = \delta_c, \qquad \text{at } x = \ell \qquad [7b]$$

where δ_c, the maximum displacement in the ligament corresponding to its failure, is independent of the size of bridging zone but varies with the area fraction, f, of ligaments. Thus, assuming that a partially-bridged crack, with $f < 1$, is analogous to a fully-bridged crack with an effective thickness of f times the full specimen thickness, Eq. [4] becomes:

$$\sqrt{\frac{\delta_c rbE'\sigma_y}{d(\ell + rb)}} = K_a + \frac{\sqrt{2}}{\pi}\int_0^{\ell} \frac{\sigma(x)\,dx}{\sqrt{x}} \qquad [8]$$

yielding an expression for the stress, $\sigma(x)$, in the ligaments:

$$\sigma(x) = -\frac{\pi}{2\sqrt{2}}\sqrt{\frac{\delta_c rbE'\sigma_y}{d}}\left[\frac{x^{1/2}}{(x + rb)^{3/2}}\right] \qquad [9]$$

With substitution, Eq. [9] provides an expression for the degree of crack-tip shielding due to uncracked-ligament bridging, in terms of the area fraction of ligaments, the applied stress intensity, and the ratio ℓ/rb:

$$K_s = -fK_a[(1 + \ell/rb)^{1/2} - 1] \div [1 - f + f(1 + \ell/rb)^{1/2}] \qquad [10]$$

C. *Limiting Strain Approach*

An alternative, first-order solution to Eqs. [2] through [4] can be obtained by representing the bridges as tensile

Table III. Force-Separation Functions for Various Models

	Marshall, Cox, Evans	Mai, Lawn	Kunz-Douglass, Beaumont, Ashby	Gerberich	Rosenfield, Majumdar
Separation-function	$\sigma(x) = 2 \cdot [u \cdot \tau \cdot E_f \cdot (1 + \eta)/R]^{1/2}$ τ: interfacial stress E_f: fiber modulus R: fiber radius η: $E_f V_f / E_m(1 - V_f)$	$p(u) = p^*(1 - u/u^*)^m$ u^*, p^*: limiting values m: mechanism-dependent $p = f \cdot \sigma(x)$	$\sigma = G \cdot (\varepsilon - 1/\varepsilon^2)$ G: modulus ε: true strain	$\sigma = \sigma_y$	$\sigma = \sigma_f$
Method	pull-out mechanics (strain compatibility)	trial function	constitutive equation for rubber	yield strength	fracture stress
Applications	fiber bridging in ceramic matrix composites	interfacial bridging	rubber-toughened plastics	general	

ligaments, where the stress in a ligament is proportional to the strain. The extent of the bridging zone then is determined by the limiting strain in the ligament farthest away from the crack tip being equal to the fracture strain. With reference to Figure 6, the strain $\varepsilon(x)$ in any ligament within the bridging zone can be estimated by assuming it to be equivalent to the strain in a bent beam, with rotational center at point C and neutral plane at the crack tip, such that:

$$\varepsilon(x) = x/rb \qquad [11]$$

Converting to a true strain and substituting into a constitutive law for the uncracked-ligament material of the form:

$$\sigma(x) = \sigma_y + k\varepsilon(x) \qquad [12]$$

where σ_y is the (initial) yield stress and k is a constant, provides a second expression for the degree of crack-tip shielding due to uncracked-ligament bridging in terms of the area fraction of ligaments, the ratio ℓ/rb, and the (constrained) flow properties of the ligament:

$$K_s = -f \cdot \sigma_y \cdot \frac{2\sqrt{2\ell}}{\pi} \left\{ 1 + \frac{k}{\sigma_y} \left[\ln\left(1 + \frac{\ell}{rb}\right) + 2\left(\sqrt{\frac{rb}{\ell}} \tan^{-1} \sqrt{\frac{\ell}{rb}} - 1 \right) \right] \right\} \qquad [13]$$

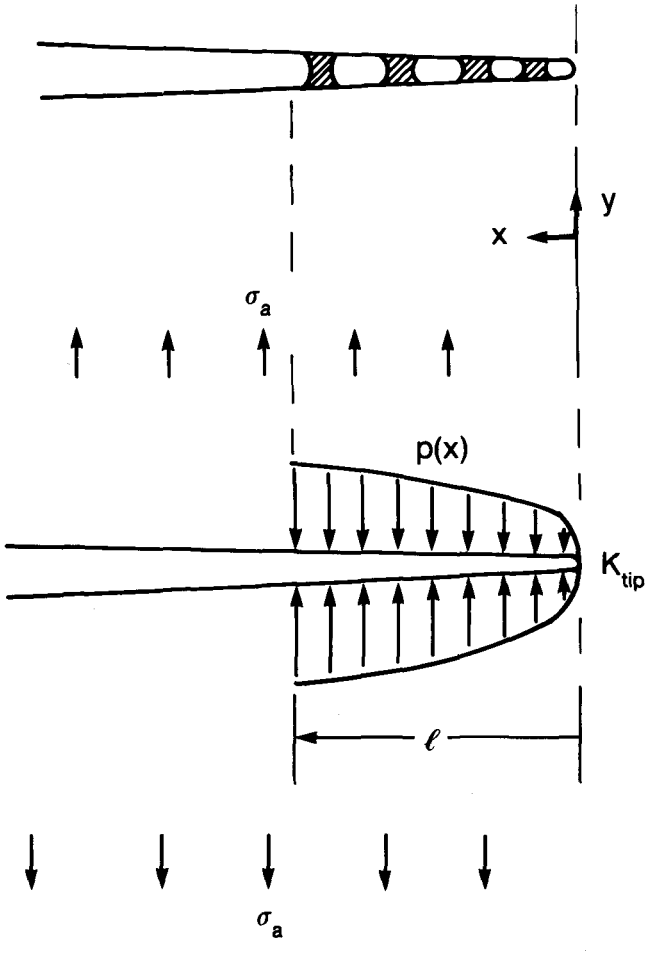

Fig. 5—Idealization of the bridging zone over distance ℓ behind the tip of a crack subjected to an externally applied stress σ_a.

VI. DISCUSSION

To evaluate the proposed expressions for crack bridging in Eqs. [10] and [13], we note that the phenomenon

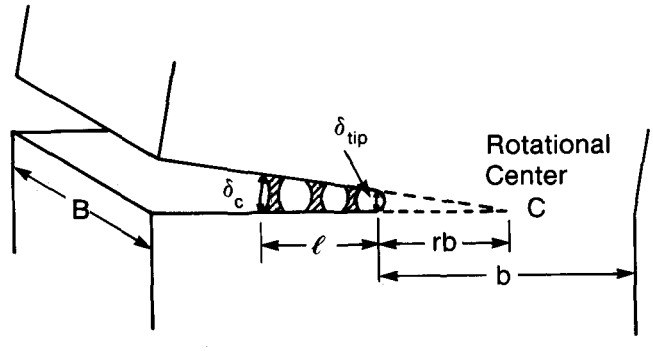

Fig. 6—Schematic illustration of idealized fatigue crack with bridging zone, showing definitions of the rotational center and crack-opening displacements.

predominates in the Al/SiC_p alloys between $\sim 10^{-9}$ and 10^{-6} m/cycle. Measurements over this range, involving metallographic studies of the crack-path morphology using serial sectioning at an average stress-intensity range ΔK of approximately 8 MPa$\sqrt{m}$ (K_a = 9 MPa$\sqrt{m}$), indicated an area fraction of bridges of 27 to 31 pct along a bridging zone, ℓ, of approximately 400 μm behind the crack tip; rb is typically 1 mm for the $DB(M_2)$ geometry. The constitutive properties of the bridges pertain to deformation under highly constrained conditions. However, in the absence of such information, properties determined uniaxially are assumed; thus, values of σ_y and k are taken, respectively, to be 380 and 1600 MPa for unreinforced bridges, and 405 and 2200 MPa for reinforced bridges.

A. *Specific Trends*

Some specific trends in the degree of crack-tip shielding predicted by Eqs. [10] and [13] are plotted in Figures 7 and 8. The influence of the size of the bridging zone is shown for both models in Figure 7 where the normalized shielding stress intensity, K_s/K_a, is plotted as a function of ℓ/rb. For Eq. [13], K_s is normalized by the shielding stress intensity, K'_a, evaluated where the uniform stress in all ligaments is equal to the yield stress.[15]

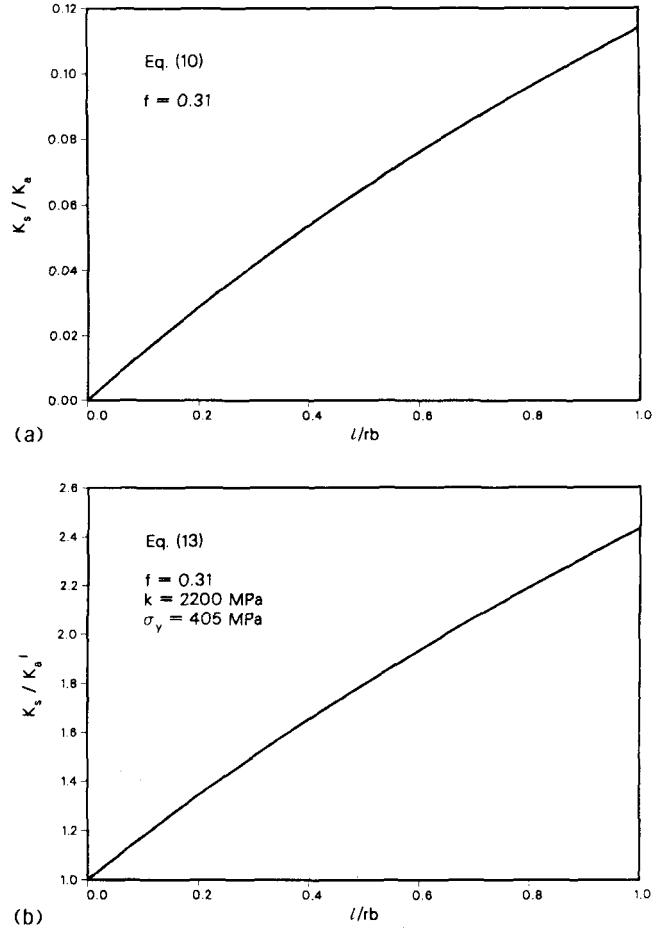

Fig. 7—*Predictions of normalized shielding stress intensity, K_s/K_a, as a function of normalized bridging-zone length, ℓ/rb, from (a) limiting crack-opening displacement (Eq. [10]); (b) limiting-strain (Eq. [13]) crack-bridging models.*

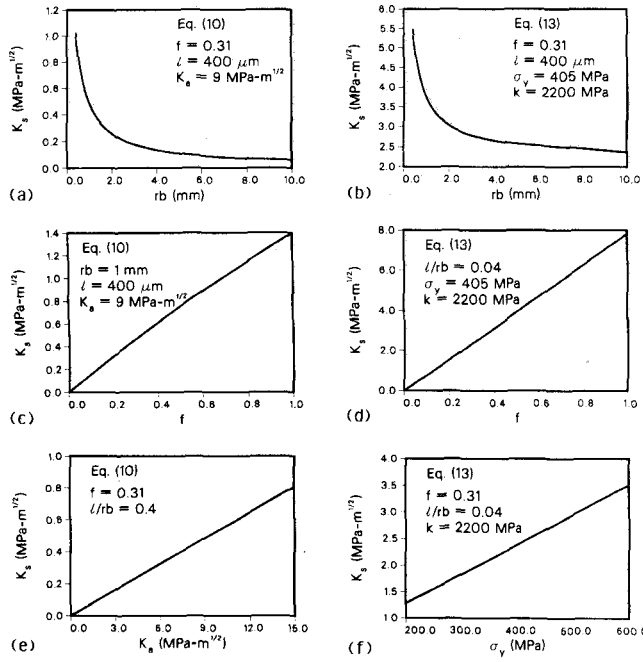

Fig. 8—*Predictions of the shielding stress intensity, K_s, as a function of (a) and (b) rb; (c) and (d) area fraction of uncracked ligaments, f; (e) applied stress intensity, K_a; (f) yield strength, σ_y, of ligament material; (a), (c), and (e) are based on limiting crack-opening displacement model (Eq. [10]); (b), (d), and (f) are based on limiting-strain (Eq. [13]) model.*

Clearly for both models, K_s increases monotonically with ℓ/rb; specifically, K_s tends to zero as ℓ approaches zero, and at a finite bridging-zone size, K_s increases with ℓ in a nearly parabolic fashion, consistent with the previous models[14,15] which utilize different stress/separation functions. The dependence of K_s on rb in both equations is hyperbolic (Figures 8(a) and (b)) and may be taken as a consequence of the assumed crack geometry. However, since rb is related to the crack-opening angle (COA) by:

$$\text{COA} = \tan^{-1}(\delta_{tip}/2rb) \qquad [14]$$

this dependence is expected for crack extension at constant COA,[39] as δ_{tip} must decrease with decreasing rb; as rb approaches zero, δ_{tip} must be zero for a finite COA, leading to $K_{tip} = 0$ or $K_s = K_a$, which is the limiting case for Eq. [10] as $rb \rightarrow 0$.

The effect of varying the area fraction of uncracked ligaments, as predicted from Eqs. [10] and [13], is plotted in Figures 8(c) and (d). Whereas both models yield the obvious limiting case of $K_s \rightarrow 0$ as $f \rightarrow 0$, for the other limit of $f \rightarrow 1$, which corresponds to a fully bridged crack, Eq. [10] yields a simple upper bound; the crack-opening displacement at the end of the bridging zone along a crack of length (a) is determined by the stress intensity ahead of a crack of length ($a - \ell$). Using Eq. [5], this implies:

$$K_{tip} = K_{a-\ell}\left(\frac{rb}{\ell + rb}\right)^{1/2} \qquad [15]$$

such that:

$$K_s = K_{tip} - K_a = -K_a\left[1 - \frac{K_{a-\ell}}{K_a} \cdot \left(1 + \frac{\ell}{rb}\right)^{-1/2}\right] \qquad [16]$$

which is consistent with the same limit in Eq. [10] provided $\ell/a \ll 1$:

$$K_s = -K_a[1 - (1 + \ell/rb)^{-1/2}] \qquad [17]$$

Finally, for fixed values of f and ℓ/rb, the shielding stress intensity K_s is predicted to show a linear dependence on both applied stress intensity and yield strength, as illustrated in Figures 8(e) and (f).

B. *Application to Al/SiC$_p$ Composites*

To apply these models to the cyclic crack-growth behavior in Al/SiC$_p$ composites (Figure 2), we note that the stretching of coplanar uncracked ligaments is controlled by the crack opening; thus, the degree of crack-tip shielding is described more appropriately by the limiting crack-opening displacement model (Eq. [10]). Using the measured values of f, ℓ, and rb defined above, the stress intensity K_s due to bridging is predicted to be approximately 0.5 MPa$\sqrt{m}$ at an applied K_a of 9 MPa$\sqrt{m}$. This form of bridging thus induces minimal shielding (~6 pct in this case), consistent with the minimal difference in growth rates between the reinforced and unreinforced 20 vol pct SiC alloys at $\Delta K = 8$ MPa$\sqrt{m}$ (Figures 2(a) and (b)). Conversely, the deformation of uncracked ligaments resulting from overlapping cracks is less a function of the crack opening, but rather is limited by the strength of the ligament; therefore, the limiting-strain model (Eq. [13]) is more appropriate. Here, using measured values of f, ℓ, rb, σ_y, and k at $K_a = 9$ MPa$\sqrt{m}$, the stress intensty K_s due to bridging is predicted to be ~2.4 MPa$\sqrt{m}$ for reinforced ligaments and ~3.2 MPa$\sqrt{m}$ for unreinforced ligaments. This clearly represents a more substantial degree of shielding (~25 to 30 pct) and is consistent with the larger shift in growth-rate curves between the reinforced and unreinforced 15 vol pct SiC alloys at $\Delta K = 8$ MPa$\sqrt{m}$ (Figures 2(c) and (d)).

It should be noted that such direct application of the bridging models to account for differences in the growth-rate behavior of the unreinforced and reinforced alloys is complicated by the simultaneous action of several mechanisms (Figure 9). For example, growth rates will be influenced additionally by such processes as limited carbide fracture ahead of the tip, crack deflection, and resulting crack closure from fracture-surface asperity contact.[17] However, crack closure from asperity-wedging predominates at near-threshold levels where the crack-opening displacements are comparable to the asperity size;[40] in contrast, the influence of uncracked-ligament bridging essentially is insignificant in this regime. This follows not simply from the mathematics which predict $K_s \to 0$ as $K_a \to 0$ (Figure 8(e)), but from the fact that the uncracked ligaments result primarily from fracture events triggered ahead of the crack tip; *e.g.*, SiC-particle fracture, which is favored only at higher stress-intensity levels.[17] This can be best explained in statistical terms. The maximum probability of a particle fracture always is located some distance ahead of the tip, because although the stresses are highest very close to the tip, the probability of finding a larger, more crackable particle increases with the sampling volume, *i.e.*, with distance

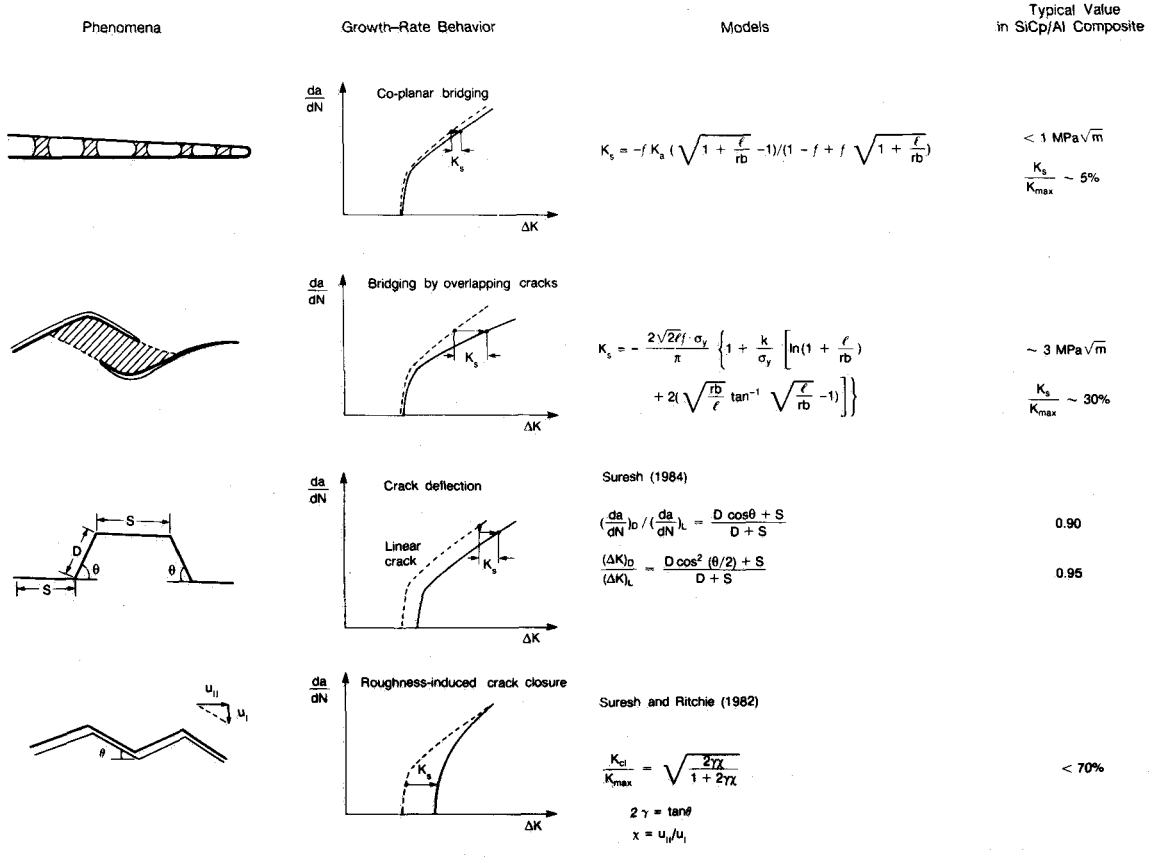

Fig. 9—Schematic illustration of primary mechanisms, models, and implications of crack-tip shielding in metal-matrix composites.

Table IV. Plastic-Zone and Particle Dimensions in Al/SiC_p Composites

Alloy	Average Particle Size (μm)	Average Particle Spacing (μm)	Plastic-Zone Size* ΔK_{TH} (μm)	Plastic-Zone Size* $\Delta K = 8$ MPa$\sqrt{m}$ (μm)
MB78 + 15 pct coarse SiC_p	11.4	56	15	77
MB78 + 20 pct fine SiC_p	6.1	23	12	81

*Estimated from $(1/2\pi)\ (K_{max}/\sigma_y)^2$.

ahead of the crack tip within the plastic zone.[17,29,30] Although expressions for the sampling volume[30] are beyond the scope of this paper, upper-bound estimates can be made from the cube of the plastic-zone size; computations of the plastic-zone size are listed for the two Al/SiC_p composite alloys in Table IV. It is apparent that at near-threshold levels, the radius of sampling volume is comparable to the average particle size and much less than the particle spacing; thus, extensive SiC particle fracture ahead of the crack tip, and hence the consequent production of uncracked ligaments, are extremely unlikely. However, as the stress intensity is raised, the generation of crack bridges becomes significant as the sampling volume increases rapidly in actuality with the sixth power of the stress intensity.

Finally, it might be noted that the toughening induced by coplanar uncracked ligaments can be viewed in two different ways: as crack bridging by ligaments in the crack wake, if the crack is considered to encompass all of the disconnected coplanar microcracks with the tip at the leading microcrack (as above) or as shielding derived from the growth of microcracks in a damage zone ahead of the crack tip, which then is associated with the point of crack continuity, *i.e.*, of failure of the last bridging element. The distinction, whether the ligaments constitute a bridging zone *behind* the crack tip (which appears beneficial to hindering crack advance) or a damage zone *ahead* of it (which would appear detrimental), depends solely on the definition of the crack tip. However, this apparent paradox has recently been treated in some detail by Thouless, who finds that the two approaches are actually equivalent and that identical crack-extension rates are predicted.[41]

VII. CONCLUSIONS

Based on a study of crack bridging *via* uncracked ligaments in P/M Al-Zn-Mg-Cu alloys reinforced with 15 to 20 vol pct of silicon carbide particulate (Al/SiC_p), simple models are developed to predict the magnitude of crack-tip shielding during fatigue-crack growth. It is found that the production of uncracked ligaments is associated with fracture events triggered ahead of the crack tip, specifically the cracking of SiC particles; as such particle fractures are significant only at higher stress-intensity levels, crack bridging is seen to predominate at higher growth rates, typically between 10^{-9} and 10^{-6} m/cycle. Proposed crack-bridging models based upon a limiting crack-opening displacement in the bridge are found to predict only minimal shielding, but are most appropriate to coplanar ligaments. Conversely, models based on a limiting strain are appropriate to ligaments formed by overlapping cracks, and predict larger levels of shielding, consistent with experimental results.

APPENDIX

Macrocrack/microcrack interaction: local stress-intensity solutions

For a collinear microcrack, length $2c$, located at distance D directly ahead of a semi-infinite macrocrack (Figure A1(a)), the local stress-intensity factors at the macrocrack tip, O, and macrocrack tips, A and B, are given in terms of the macrocrack stress-intensity factor (in the absence of the microcrack) $K_I(\infty)$ by Rubinstein[31] as:

$$\frac{K_I(O)}{K_I(\infty)} = \sqrt{\frac{D+2c}{D}}\ \frac{\Sigma\left[1-\left(\frac{D}{D+2c}\right)\right]}{\Gamma\left[1-\left(\frac{D}{D+2c}\right)\right]}$$

$$\frac{K_I(A)}{K_I(\infty)} = \left\{\frac{D+2c}{D}\cdot\frac{\Sigma\left[1-\left(\frac{D}{D+2c}\right)\right]}{\Gamma\left[1-\left(\frac{D}{D+2c}\right)\right]} - 1\right\} \div \sqrt{\frac{2c}{D}} \qquad [A\text{-}1]$$

and

$$\frac{K_I(B)}{K_I(\infty)} = \left\{1 - \frac{\Sigma\left[1-\left(\frac{D}{D+2c}\right)\right]}{\Gamma\left[1-\left(\frac{D}{D+2c}\right)\right]}\right\} \div \sqrt{1-\left(\frac{D}{D+2c}\right)} \qquad [A\text{-}2]$$

where the first and second complete elliptic integrals Γ and Σ are given by:

$$\Gamma(g) = \int_0^{\pi/2} \frac{d\theta}{\sqrt{1-g^2\sin^2\theta}}$$

and

$$\Sigma(g) = \int_0^{\pi/2} \sqrt{1-g^2\sin^2\theta}\, d\theta$$

Note Eq. [A-2] has been modified to correct an error in the original paper.[31]

In the present case of fatigue-crack growth in Al/SiC_p composites, where the region of microcracks is bounded by the plastic-zone size and, therefore, is only ~5 to 15

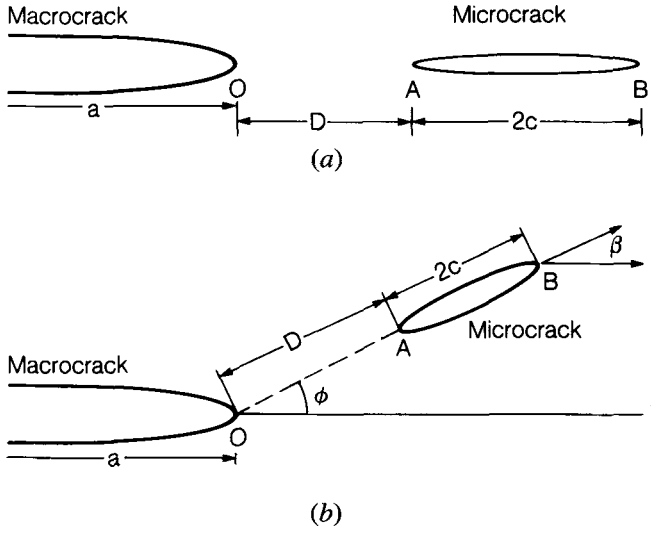

Fig. A1—Geometry of macrocrack/microcrack interaction for (*a*) coplanar; (*b*) off-angle microcracks.

times larger than the particle size, Eqs. [A-1] and [A-2] are evaluated at $D/2c$ values of order unity. The presence of the microcrack leads to an increase in the stress intensity at the macrocrack tip, $K_I(O)$, of up to 23 pct; conversely, the stress intensity at the microcrack tip A, $K_I(A)$, is increased by up to 74 pct of the far-field $K_I(\infty)$ acting on the macrocrack.

For arbitrarily inclined microcracks located ahead of a macrocrack (Figure A1(b)), the local stress-intensity factors are a complex function of the relative size and position of the microcrack.[32,33,34] For the same case of $D/2c$ of order unity, the corresponding elevation of the stress intensity at the macrocrack tip, $K_I(O)$, is now reduced to only ~2 pct; the stress intensity at the microcrack tip, $K_I(A)$, however, is enhanced by ~40 pct, representing a 100 pct increase over the stress intensity in the absence of the macrocrack (for $\varphi = \beta = \pi/5$, $a = 25c$).

These solutions must be considered approximate as they pertain to two-dimensional cracks; conversely, the microcracks generated in the Al/SiC_p composites are not continuous through the specimen thickness.

NOMENCLATURE

a	(macro) crack length
b	uncracked specimen ligament
c	half length of microcrack
C	constant in Eq. [1]
COA	crack-opening angle
d	constant in Eq. [6]
da/dN	fatigue-crack growth rate per cycle
$dp(x)$	distributed force per unit thickness (Eq. [2])
D	distance of microcrack from macrocrack tip
E	Young's modulus
E'	$= E/(1 - \nu^2)$ in plane strain, and E in plane stress
E_f, E_m	fiber and matrix modulus, respectively
f	area fraction of uncracked ligaments on crack plane
g	variable in elliptic integrals
G	shear modulus
G_c	critical strain energy release rate (toughness)
k	constant in constitutive law (Eq. [12])
K	stress-intensity factor
K_a, $K_I(\infty)$	applied stress intensity
$K_{a-\ell}$	stress intensity ahead of crack of length $(a - \ell)$
K_{cl}	closure stress intensity
K_{Ic}	plane-strain fracture toughness
$K_{\max}$, $K_{\min}$	maximum and minimum stress intensity, respectively
K_s	shielding stress intensity
K_{tip}	near-tip stress intensity
ΔK	(nominal) stress-intensity range $(=K_{\max} - K_{\min})$
ΔK_{eff}	effective stress-intensity range $(=K_{\max} - K_{cl})$
ΔK_{TH}	(measured) fatigue-crack growth threshold
$\Delta K_{TH,\text{eff}}$	intrinsic (effective) fatigue-crack growth threshold
ℓ	length of bridging zone
m	exponent
$p(x)$	bridging force in ligaments
r	rotational factor
R	load ratio $(=K_{\min}/K_{\max})$
R_f	radius of reinforcement-phase particle
u	displacement
V_f	volume fraction of reinforcement phase
x, y	coordinates, with origin at the crack tip
Γ, Σ	first and second complete elliptic integrals, respectively
δ_c	critical crack-opening displacement (at K_{Ic})
δ_{tip}	crack-tip opening displacement
δ_x	crack-opening displacement at distance x from the tip
ε	(true) strain
$\varepsilon(x)$	strain in ligament
ν	Poisson's ratio
φ, β	angles associated with microcrack and macrocrack orientations
σ	stress
σ_a	applied stress
σ_f	fracture stress
$\sigma(x)$	stress in ligament
σ_y	yield strength
τ	interfacial stress
θ	dummy variable

ACKNOWLEDGMENTS

This work was supported by the Air Force Office of Scientific Research under University Research Initiative No. F49620-87-C-0017 to Carnegie Mellon University. Thanks are due to Dr. Alan Rosenstein for his continued support, to Warren Hunt and Dr. Bob Bucci of Alcoa for supplying the alloys, to Larry Edelson for help in characterizing the microstructures, and to Madeleine Penton for her assistance in preparing the manuscript.

REFERENCES

1. A.G. Evans: in *Fracture Mechanics*, 20th Symp., ASTM STP, R.P. Wei and R.P. Gangloff, eds., American Society for Testing and Materials, Philadelphia, PA, 1989.
2. R.O. Ritchie: *Mater. Sci. Eng. A*, 1988, vol. 103, pp. 15-28.
3. J. Aveston, G. Cooper, and A. Kelly: in *Properties of Fiber Composites*, NPL Conf. Proc., IPC Sci. & Tech. Press, Surrey, U.K., 1971, pp. 15-26.
4. B. Budiansky, J.W. Hutchinson, and A.G. Evans: *J. Mech. Phys. Solids*, 1986, vol. 34, pp. 167-89.
5. D.B. Marshall, B.N. Cox, and A.G. Evans: *Acta Metall.*, 1985, vol. 33, pp. 2013-21.
6. L.N. McCartney: *Proc. Roy. Soc.*, 1987, vol. A409, pp. 329-50.
7. L.R.F. Rose: *J. Mech. Phys. Solids*, 1987, vol. 35, pp. 383-405.
8. B. Budiansky: in *Proc. 10th U.S. Cong. Appl. Mech.*, Austin, TX, 1986.
9. S. Kunz-Douglass, P.W.R. Beaumont, and M.F. Ashby: *J. Mater. Sci.*, 1980, vol. 15, pp. 1109-23.
10. A.G. Evans, Z.B. Ahmad, D.G. Gilbert, and P.W.R. Beaumont: *Acta Metall.*, 1986, vol. 34, pp. 79-87.
11. A.G. Evans and R.M. McMeeking: *Acta Metall.*, 1986, vol. 34, pp. 2435-41.
12. L.R.F. Rose: *Mech. Mater.*, 1987, vol. 6, pp. 11-15.
13. P.L. Swanson, C.J. Fairbanks, B.R. Lawn, Y. Mai, and B.J. Hockey: *J. Am. Ceram. Soc.*, 1987, vol. 70, pp. 279-89.
14. Y. Mai and B.R. Lawn: *J. Am. Ceram. Soc.*, 1987, vol. 70, pp. 289-94.
15. W.W. Gerberich: in *Fracture: Interactions of Microstructure, Mechanism and Mechanics*, J.M. Wells and J.D. Landes, eds., TMS-AIME, Warrendale, PA, 1984, pp. 49-74.
16. A.R. Rosenfield and B.S. Majumdar: *Metall. Trans. A*, 1987, vol. 18A, pp. 1053-59.
17. J.-K. Shang, W. Yu, and R.O. Ritchie: *Mater. Sci. Eng. A*, 1988, vol. 102, pp. 181-92.
18. R. Marissen: in *Fatigue 87*, Proc. 3rd Int. Conf. on Fatigue, R.O. Ritchie and E.A. Starke, eds., EMAS Ltd., Warley, U.K., 1988, vol. 3, pp. 1271-79.
19. R.O. Ritchie, W. Yu, and R.J. Bucci: *Eng. Fract. Mech.*, 1989, in press.
20. T. Christman and S. Suresh: *Mater. Sci. Eng. A*, 1988, vol. 102, pp. 211-16.
21. J.J. Lewandowski, C. Liu, and W.H. Hunt: in *Powder Metallurgy Composites*, M. Kumar, K. Vedula, and A.M. Ritter, eds., TMS-AIME, Warrendale, PA, 1987.
22. J.E. Srawley and B. Gross: *Mat. Res. Stand.*, 1967, vol. 7, pp. 155-62.
23. R.O. Ritchie and W. Yu: in *Small Fatigue Cracks*, R.O. Ritchie and J. Lankford, eds., TMS-AIME, Warrendale, PA, 1986, pp. 167-89.
24. R.O. Ritchie, J.F. Knott, and J.R. Rice: *J. Mech. Phys. Solids*, 1973, vol. 21, pp. 395-410.
25. J.W. Hutchinson: *J. Mech. Phys. Solids*, 1968, vol. 16, pp. 13-31.
26. J.R. Rice and G.R. Rosengren: *J. Mech. Phys. Solids*, 1968, vol. 16, pp. 1-12.
27. J.R. Rice and M.A. Johnson: in *Inelastic Behavior of Solids*, M.F. Kanninen, W.G. Adler, A.R. Rosenfield, and R.I. Jaffee, eds., McGraw-Hill, New York, NY, 1970, pp. 641-72.
28. R.M. McMeeking: *J. Mech. Phys. Solids*, 1977, vol. 24, pp. 357-19.
29. T. Lin, A.G. Evans, and R.O. Ritchie: *J. Mech. Phys. Solids*, 1986, vol. 34, pp. 477-97.
30. T. Lin, A.G. Evans, and R.O. Ritchie: *Metall. Trans. A*, 1987, vol. 18A, pp. 641-51.
31. A.A. Rubinstein: *Int. J. Fract.*, 1985, vol. 27, pp. 113-19.
32. H. Horii and S. Nemat-Nasser: *Int. J. Solids Struct.*, 1985, vol. 21, pp. 731-45.
33. M. Hori and S. Nemat-Nasser: *J. Mech. Phys. Solids*, 1987, vol. 35, pp. 601-29.
34. A. Chudnovsky, A. Dolgopolsky, and M. Kachanov: in *Advances in Fracture Research*, Proc. 6th Int. Conf. on Fracture, India, S.R. Valluri *et al.*, eds., Pergamon Press, Oxford, 1984, vol. 2, pp. 825-32.
35. G.C. Sih: *Handbook of Stress Intensity Factors*, Lehigh University Press, Bethlehem, PA, 1972.
36. J.-L. Tzou, C.H. Hseuh, A.G. Evans, and R.O. Ritchie: *Acta Metall.*, 1985, vol. 33, pp. 117-27.
37. C.C. Veerman and T. Muller: *Eng. Fract. Mech.*, 1972, vol. 4, pp. 25-32.
38. C.F. Shih: *J. Mech. Phys. Solids*, 1981, vol. 29, pp. 305-30.
39. J.R. Rice: in *Mechanics and Mechanisms of Crack Growth*, M.J. May, ed., British Steel Corp., London, U.K., 1974, pp. 14-39.
40. S. Suresh and R.O. Ritchie: *Metall. Trans. A*, 1982, vol. 13A, pp. 1627-31.
41. M.D. Thouless: *J. Am. Ceram. Soc.*, 1988, vol. 71, pp. 408-13.